LLNL-TR-833544

Lawrence Livermore National Laboratory

Characterization, chemistry, and particle size distribution of fallout particles isolated from filter samples

Maryline Kerlin, Enrica Balboni, Kim Knight

March 28th, 2022

Disclaimer

Lawrence Livermore National Laboratory is operated by Lawrence Livermore National Security, LLC, for the U.S. Department of Energy, National Nuclear Security Administration under Contract DE-AC52-07NA27344.

Funding: LDRD 20-SI-006: Post-Detonation Chemical Behavior in Complex Environments

Abstract

Nuclear particulate fallout is the radioactive byproduct of a nuclear event formed by the mixture of proximate environmental materials with vaporized bomb debris. The debris can be transported into the atmosphere during cloud rise, raining out locally and globally constituting a radiation hazard. Questions remain on how entrainment of environmental material in the fireball affects fallout formation processes and radionuclide incorporation during cooling.

Here we analyzed an archived air filter collected from an aircraft in the aftermath of ground interacting US nuclear tests. Chemical information on particles composition was obtained from Scanning Electron Microscopy coupled with Energy Dispersive X-ray Spectroscopy (SEM-EDS) and Infrared (IR) spectroscopy. The particle size distribution was obtained using Dynamic Light Scattering (DLS) technique and analyses of SEM images.

Experimental section

1. Sample preparation

An approximately 5 x 7 cm cut section of a filter paper (see Fig. 1.a) was placed in a quartz crucible and heated in a box furnace to achieve the decomposition of the organic material (filter). The heating profile of the experiment was as follows: starting at room temperature, the temperature was increased to 650 °C and held for 12 h, the furnace then was then cooled to 25 °C at a ~1 °C/min cooling rate. The residue obtained after heat treatment was transferred to a vial with 5 mL of ethanol (see Fig. 1.b). The sample was then diluted and homogenized by manual stirring (i.e., pipetting in and out the solution). This suspension was used to perform chemical characterization and particles size distribution measurements as discussed below.
Prior to heating, a fragment of the cut filter paper (0.5 x 0.5 cm) was saved and prepared for imaging via Scanning Electron Microscope (SEM). A sample was prepared from the fragment as follows: carbon tape was placed onto a SEM stub, and the carbon tape side was placed against the filter to pick up some fibers containing particles. The sample was then carbon coated to improve imaging quality by SEM.

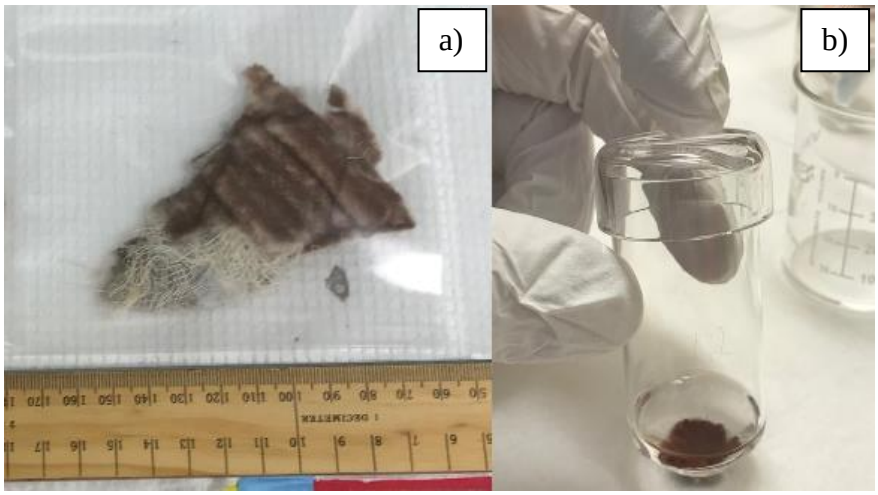

Fig. 1. Pictures taken showing sample FLD-20-01-12 at different stages, a) cut section of the filter, b) filter residue obtained after heating process in box furnace. No obvious change in color of the particles was observed, particles trapped in the white filter paper have the same color (red/brown) as the particles isolated from the filter.

2. Chemical characterization

SEM-EDS analysis

A dilute sample aliquot dispersed in ethanol was homogenized by using a vortex mixer. The sample solution was sonicated for 5 minutes under the high setting, and 1 small drop of solution was deposited onto carbon tape placed on a SEM stub and carbon coated after drying.
All SEM-EDS analyses were performed using a FEI Inspect F SEM operating at 20 kV with a spot size of 5 and a working distance of 11.5 ± 0.1 mm. The instrument is equipped with an Everhart-Thornley secondary electron detector (ETD) and a solid-state backscattered electron detector (BSED). The SEM is also outfitted with a Bruker XFlash 6160 60 mm^2 silicon drift detector to perform energy dispersive spectrometry (EDS). Semi quantitative SEM Energy Dispersive X-ray Spectroscopy (SEM-EDS) spot analysis were performed on about 20 particles to determine the major and minor elements composition of the particles.

IR measurements

The IR measurements were performed on an Agilent technologies Cary 630 FTIR instrument using the diamond ATR (Attenuated Total Reflectance) attachment. For the analysis an aliquot of the sample (suspended in ethanol) was placed on the diamond ATR and let to dry completely before starting the measurements. The IR spectra of various known materials (used as reference materials) were analyzed following the same procedure as the samples. Before each measurement, a background scan was collected (20 scans), prior to sample analysis. For each solid samples, 150 scans were collected between 4 000 and 650 cm^{-1}.

3. Particle size analysis

Dynamic light scattering (DLS)

DLS measurements were performed using a Zetasizer ULTRA (Malvern Instruments Ltd., GB) performed in backscattered mode (scattering collection angle is 175°) with a 632.8 nm laser and an attenuation factor of 8 or 9. A constant temperature of 25 °C was maintained through each measurement. To prepare samples for DLS analysis, a 20 µL aliquot of the homogenized diluted suspension in water was transferred into a new vial and further diluted with 2 mL of sucrose solution. The sample was vortexed for 1 minute and 0.9 mL of solution was transferred into a rinsed 4-clear-sided walls cleaned cuvette (10 x 10 mm).

Data analysis was performed using the ZS Xplorer Zetasizer software. In the software the dispersant was set to sucrose, with refractory index and viscosity set for 25 °C (see Table 1), and the material chosen analyzed was Fe_2O_3 (hematite; having pre-determined parameters such as refractive index of 3.13 and absorption of 0.017). Data processing was performed using Multiple Narrow Mode, which allows to account for polydisperse samples (variable size populations). Raw data from the software provided values of the mean peak position in nm and its associated area in %. In all the scans collected we observed one or two peaks. Each mean peak position was then placed in a bin (50 nm bins between 0 and 99 nm, 100 nm bins between 100 and 999 nm, and 1 000 nm bins between 1 000 and 6 000 nm) with its associated area. For each bin, the peak frequency was calculated by counting the number of peaks present in the bin and is then weighted by the % area associated to each peak.

Table 1. Parameters used in the Zetasizer software for the different dispersants studied at 25 °C. These parameters are used by the software to calculate the particle size distribution of the sample analyzed. Data given for water and 40% sucrose were already pre-determined in the software. The values for 60% and 70% sucrose solutions were obtained in reference 2 for the refractive index and in reference 3 for the viscosity given in centipoise (1 centipoise = 1 mPa.s). *Note: the references have similar data as the ones given by the software for 40% sucrose solution.*

Dispersant solution	Refractive Index	Viscosity in mPa.s
MQ H_2O	1.33	0.8872
40% sucrose	1.4	5.1178
60% sucrose	1.44	44.03
70% sucrose	1.46	321.6

Particle size analysis using SEM

All SEM images for particle size distribution analysis were collected under high vacuum ($2x10^{-5}$ and $3x10^{-6}$ mbar) using a FEI Inspect F SEM operating at 15 kV with a spot size of 4.5 and a

working distance of 11.6 ± 0.1 mm. For sample preparation, a 75 µL aliquot of the homogenized diluted suspension in water was transferred into a new vial and further diluted with 4 mL of ethanol. The sample was sonicated for 25 minutes under the high setting to promote disaggregation, then vortexed for 1 minute and manually stirred to homogenize. One small drop of the sample was taken and deposited onto carbon tape placed on a SEM stub, and carbon coated (when dry) with an approximate thickness of 13.7 ± 0.7 nm.

SEM images analyses for particle size distribution was performed manually on particles of interest (see Results section). Measurements of the particles were performed using the MAMA (Morphological Analysis for Material Attribution, see reference 1) software developed at Los Alamos National Laboratory using the ruler tool. The ruler was calibrated using the scalebar on the SEM images; a line was drawn on the line of the SEM scale and the number of pixels would be converted to micrometers associated with the scale bar (e.g., on Fig. 9 the line is 671 pixels, and the scale bar is 5 µm). No segmentation or assumptions were necessary since the measurements were performed only on spherical particles.

4. Results

Sample

Before any heat treatment, particles present on filter fibers were observed under SEM imaging in order to assess their size and morphology, the quantity of particles, the degree of particulate co-adhesion, and the presence of impurities such as soil components. As seen in Fig. 2, the sample consists of spherical particles (nanometer to micrometer size range) on fibrous material. The particles appear as both isolated particles and in agglomerated forms.

Particle size is not expected to be altered during the heating process, since originally these particles were formed under high temperature conditions. However, to confirm the hypothesis that heat treatment of the sample did not affect particle size and particle morphology, unheated particles were imaged via Scanning Electron Microscope (SEM), and observations revealed that the particles displayed similar morphological and textural features (Fig. 2 and Fig. 8). The heating of the sample to 650 °C is not expected to perturb the actinides content of the samples, due to their low volatility. Nevertheless, it may have affected the sample chemical composition due to the loss of more highly volatile elements such as iodine etc. The analysis of volatile elements was not part of the work scope of this project.

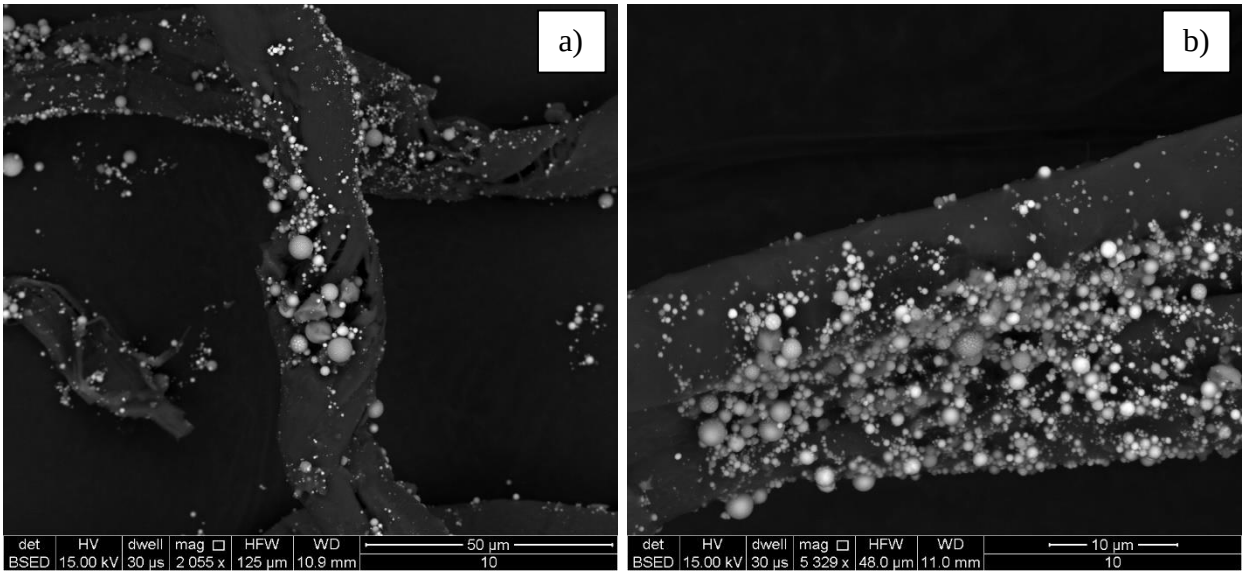

Fig. 2. Backscattered electron images of FLD-20-01-12 particles on filter fibers. High number of spherical particles are observed; size, morphological and textural features are similar to the ones observed from isolated particles in Fig. 3, 4, 7-9. Pictures a and b are taken on different fibers and at different magnifications. Picture b seems to show the presence of agglomerates.

Chemical characterization

Elemental analysis

As shown in Fig. 1.a, red/brown material is observed on one side of the filter, whereas the other side of the filter (not shown) is pristine off-white. After furnace heating the remaining residue consisted of fine grained red/brown material. SEM images revealed that the majority of the FLD-20-01-12 particles isolated from the filter are spherical and some of the particles contain some fused smaller particles (see Fig. 3 and 4).

In backscattered mode (BSE), the particles change of color (from gray to white) is indicative of compositional variation (higher Z composition appears brighter). In this sample some particles display homogenous chemical composition (uniform color) whereas other display evidence of chemical heterogeneities within each particle (shading from gray to white, Fig. 3 and 4).

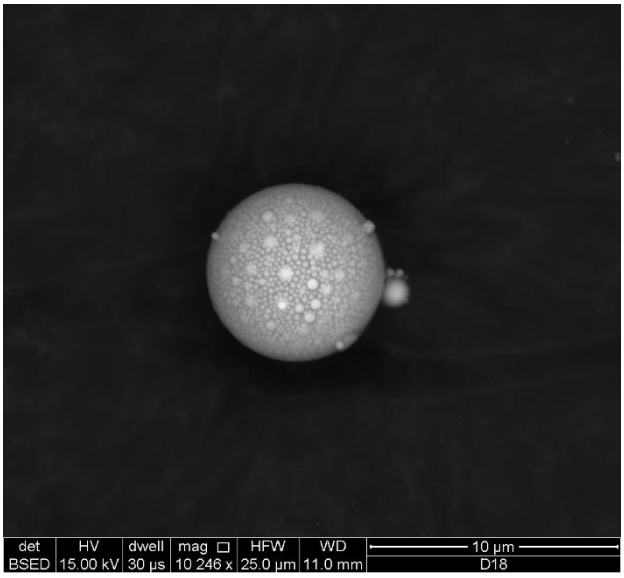

Fig. 3. Particle observed under backscattered electron imaging mode revealing heterogeneous chemical features. The particle is a darker gray matrix incorporating some white circular areas, indicating that some higher Z (atomic number) materials are dispersed in the lighter Z matrix.

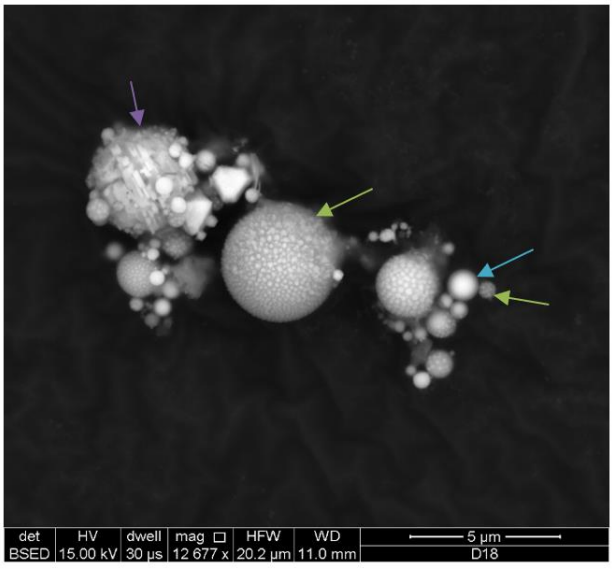

Fig. 4. Particles observed under backscattered electron imaging mode. A cyan arrow shows an example of a homogeneous particle, green arrows point to examples of a particle having chemical heterogeneities, and a purple arrow identifies a spherical particle with a compositionally textured surface.

SEM-EDS analysis of 20 particles reveals that Si, Al and Fe oxides make up between 91-97 wt.% of each analysis, however the content of these elements in each particle can vary significantly. For example, the Si content measured in about 20 particles varied between 3 to 36 wt.% (average = 13.4 ± 9.8 wt.%) and Fe content ranged from 1.5 to 29 wt.% (average = 19.9 ± 7.8 wt.%). Minor elements detected via SEM-EDS analysis included Na, Mg, K, Ca, Cu, Zr, Sn

and Pb all at ≤ 1 wt.% in each particle. Overall, the chemical analysis of these materials indicates that some particles have Al/Si-rich composition (gray color in SEM-BSE images), whereas other are more Fe-rich (white color in SEM-BSE images). EDS analyses were performed using the square tool and the pointer tool to determine specific small areas and some examples are presented in Fig. 5. No other type of particles, such as mineral grain types of material, were identified in the samples. One can note that in previous studies actinides are found in fallout particles, however their low concentrations (at ppm or trace level) would not allow to be detectable by EDS analyses.

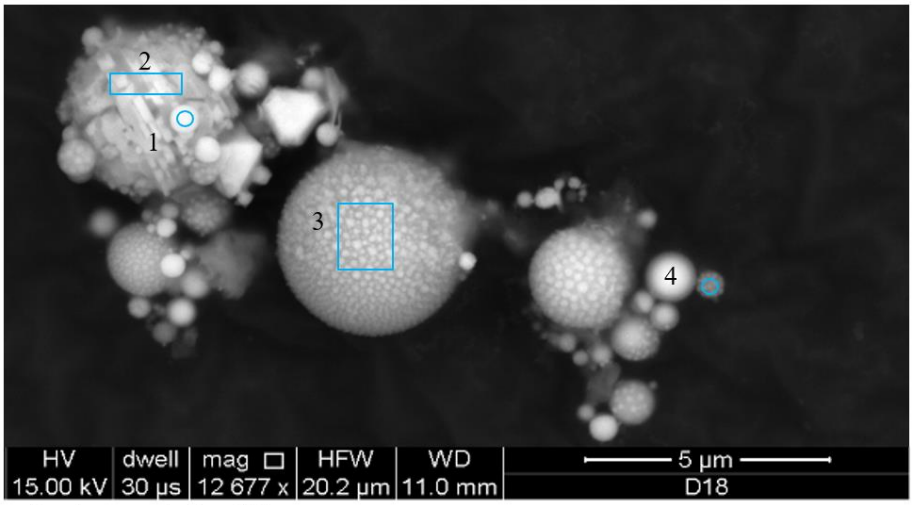

Atomic concentration [%]

Spectrum	O	Na	Mg	Al	Si	K	Ca	Ti	Mn	Fe	Cu
1	56.27	2.95	1.78	6.11	2.93	0.15	0.32	0.00	0.09	28.13	1.16
2	57.15	1.17	0.92	4.94	1.28	0.07	0.15	0.03	0.17	33.97	0.10
3	59.52	2.34	0.69	3.52	15.10	1.82	0.68	0.01	0.09	15.35	0.53
4	61.27	2.23	1.28	2.90	19.75	1.00	0.59	0.01	0.10	10.37	0.23

Fig. 5. EDS analysis of a group of particles, showing the areas analyzed: a small bright particle as a point analysis (1), a rectangle on the surface of the top left particle (2), a rectangle on the surface of the particle in the middle (3) and a small darker particle as a point analysis (4). EDS analyses show that both particles are a mixture of Si-Al-Fe oxides with some minor elements. In this image, brighter particles primarily reflect higher Fe content and lower Si content present in the particle, and vice versa for darker areas.

IR measurements

The IR spectrum of the FLD-20-01-12 particles isolated from the filter was obtained to gain some level of information about the chemical structure and characteristic chemical bonding present in the samples. Based on the chemical composition identified via SEM-EDS analyses, we measured different known materials such as iron oxide minerals (hematite, magnetite, ferrihydrite and goethite) and silicate glass (melt glass) having specific IR fingerprinting to conduct simple identification and possible match.

By comparing the spectrum of the particles isolated from the filters to the spectra of the known inorganic compounds (Fig. 6) it is apparent that FLD-20-01-12 does not contain any goethite (α-FeOOH) or ferrihydrite, since no OH peaks were observed around 3 300 – 3 000 cm^{-1} (area indicated with the grey arrow in Fig. 6). It is possible to assume that the sample may contains some magnetite (Fe_3O_4 with Fe^{+III} and Fe^{+II}) or hematite (Fe_2O_3), because of spectral similarities (< 1 000 cm^{-1}). IR spectra were collected only between 4 000 cm^{-1} and 650 cm^{-1} (instrumental limit), which unfortunately does not allow to identify differences between maghemite (γ-Fe_2O_3) and magnetite. However, compared to pristine magnetite mineral the spectrum of FLD-20-01-12 displays a peak shift around 1 200 and 900 cm^{-1} (black arrow in Fig. 6). We interpret this feature as a contribution of the silicate glass (i.e., SiO_2). EDS analyses identified that some particles are more Fe rich other more Si/Al rich, with a higher percentage of Fe present in general. IR data acquired on bulk material (vs. individual particles during EDS) is likely representative of both glassy and Fe oxides component, confirming the presence of both type of materials.

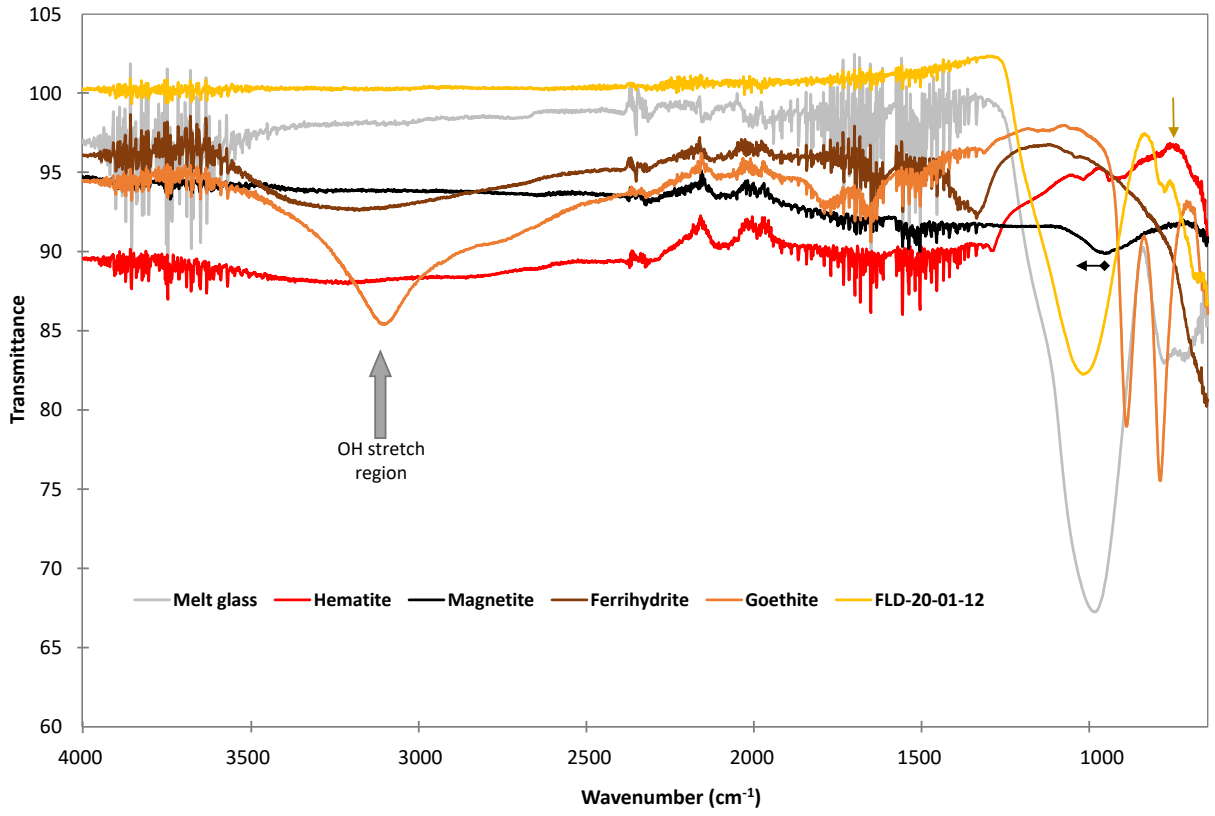

Fig. 6. IR spectra in transmittance for the standards melt glass (grey), hematite (red), magnetite (black), ferrihydrite (brown) and goethite (orange) and the particles isolated from filter FLD-20-01-12 (yellow). The grey arrow indicates the OH stretch region and the black arrow highlight the shift in the peak of magnetite and the gold arrow points at one the main peaks from hematite.

Particle size analysis

Dynamic light scattering (DLS)

Laser or light scattering instruments are commonly used to determine particle size distribution of synthetic or natural samples. Laser diffraction is a common particle sizing method especially for particles in the range of hundreds of nanometers to several millimeters. When measuring small particles (i.e., < 0.5 μm) DLS is the easiest and most common method to use. In our laboratory, the measuring range of the instrument in diameter is from 0.3 nm up to 10 μm.
DLS measurements are only performed in solution and at low concentration (i.e., to avoid multiple scattering and thus false results). A dispersant having similar density property than the particles is needed to allow having the particles in solution without floating at the surface or sinking down the cuvette (i.e., preventing the measurement).

Various tests were conducted trying to find a balance between the right concentration of particles and the best dispersant. It has been noted that during experiments ran in MQ H_2O particles were rapidly settling in the cuvette, thus hindering DLS measurements. In order to slow the deposition of heavier particles, a dispersant with similar density properties or high viscosity can be used and as a result, sucrose was selected as the dispersant of choice (Table 1).

In this report we present data obtained using 60% sucrose solution as a dispersant, prepared as described in the Experimental section. A summary of the raw data is presented in Table 2. The population size distribution was then performed as described in the Experimental section and the data is presented in Fig. 11. Two peaks were consistently identified by the DLS measurements suggesting that the sample is characterized by a bimodal distribution of particle size. The first peak, having the larger number of particles, is centered around 34.8 ± 8.4 nm and is associated with higher frequency/probability to find particles of that size range. The second peak is spread over a larger range, 778 nm to 5.07 μm, and the frequency of finding larger particles is smaller.

Table 2. Raw data obtained from 44 scans for particle size distribution via DLS. Peak mean corresponds to the mean particle size distribution for a scan, and the peak area is the area under the peak in % corresponding to a frequency of particles present under this peak. The table presents the average of peak position of all the 44 scans in nm, the associated peak area for peak 1 and peak 2 and their associated standard deviation. The minimum and maximum values represent the range of values from the experiment.

	Average	Standard deviation	Minimum value (associated Mean or Area value)	Maximum value (associated Mean or Area value)
Peak 1 Mean	34.8 nm	8.4 nm	23.4 nm (35.5%)	69.1 nm (100%)
Peak 1 Area	66.7%	25.8%	31.9% (25.7 nm)	100% for few peaks (69.1, 39.2, 37.2, 39.5, 35.6, 33.8, 42.5, 39.3, 38, 37.7, 34.1, 37.6, 37.6, 40.2, 49.3 nm)
Peak 2 Mean	1.68 μm	0.80 μm	0.78 μm (58.1%)	5.07 μm (16.2%)
Peak 2 Area	50.5%	11.0%	16.2% (5.07 μm)	68.1% (0.93 μm)

Particle size analysis using SEM images

About 30 images were analyzed to determine particle morphology and size using SE and BSE modes. The particles in the sample are present as: A) isolated spherical particles with smooth and textured surface (e.g., cyan and purple arrows in Fig. 4); B) isolated non-spherical particles (e.g., white arrows in Fig. 9 and Fig. 11); C) isolated particles with fused smaller spherical objects attached/fused to the surface (Fig. 7); and D) agglomerates containing multiple primary particles of similar sizes fused together to form a bigger secondary particle / cluster (Fig. 8 and Fig. 11). Both particles and agglomerates may display a various degree of overlapping with nearby particles which may be an artifact of sample preparation (sample dilution and/or drying).

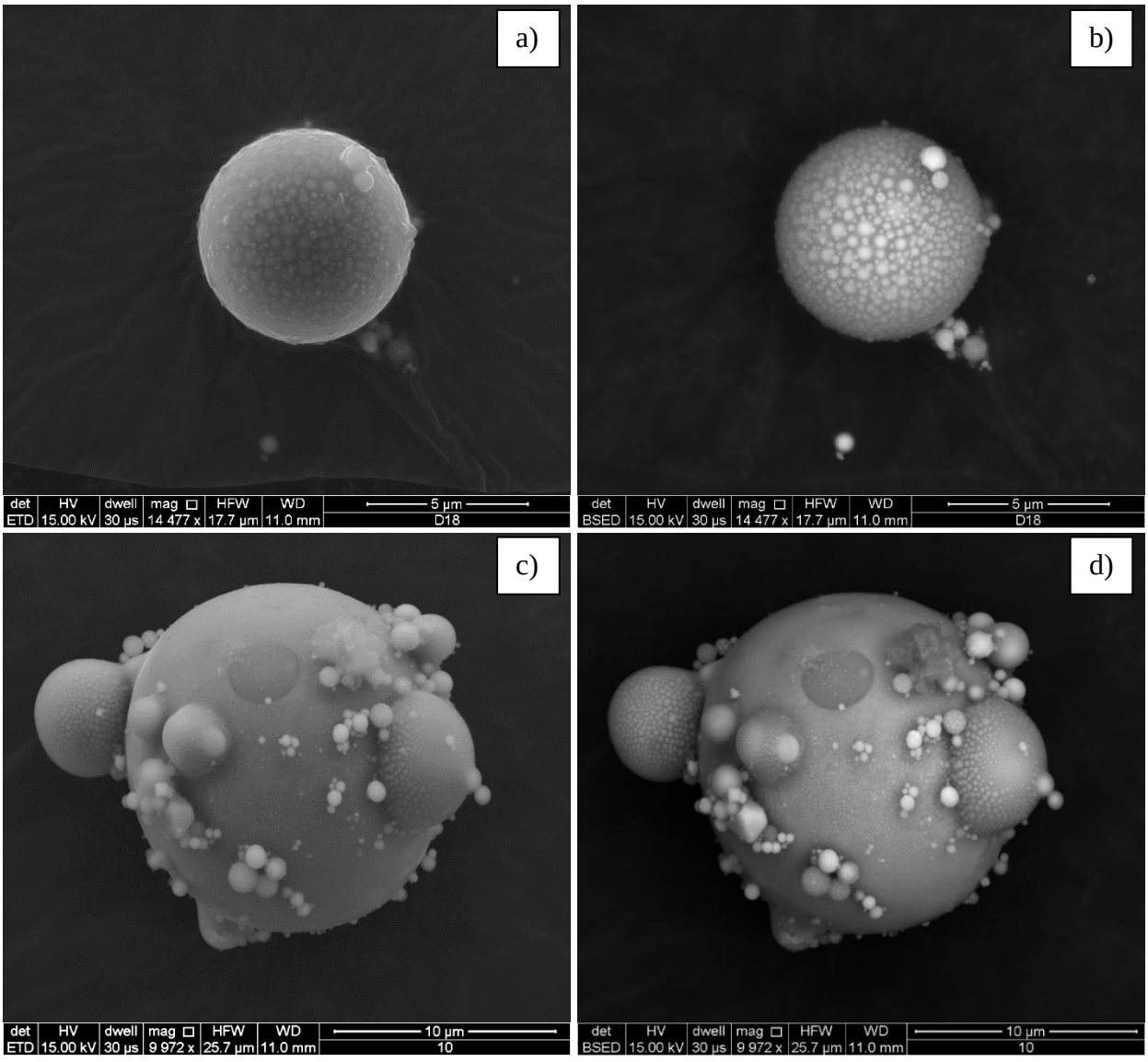

Fig. 7. Example of fused smaller particles into a bigger particle found in the ashed sample (a and b) and on filter fiber (c and d) under secondary (a and c) and backscattered (b and d) electron imaging mode.

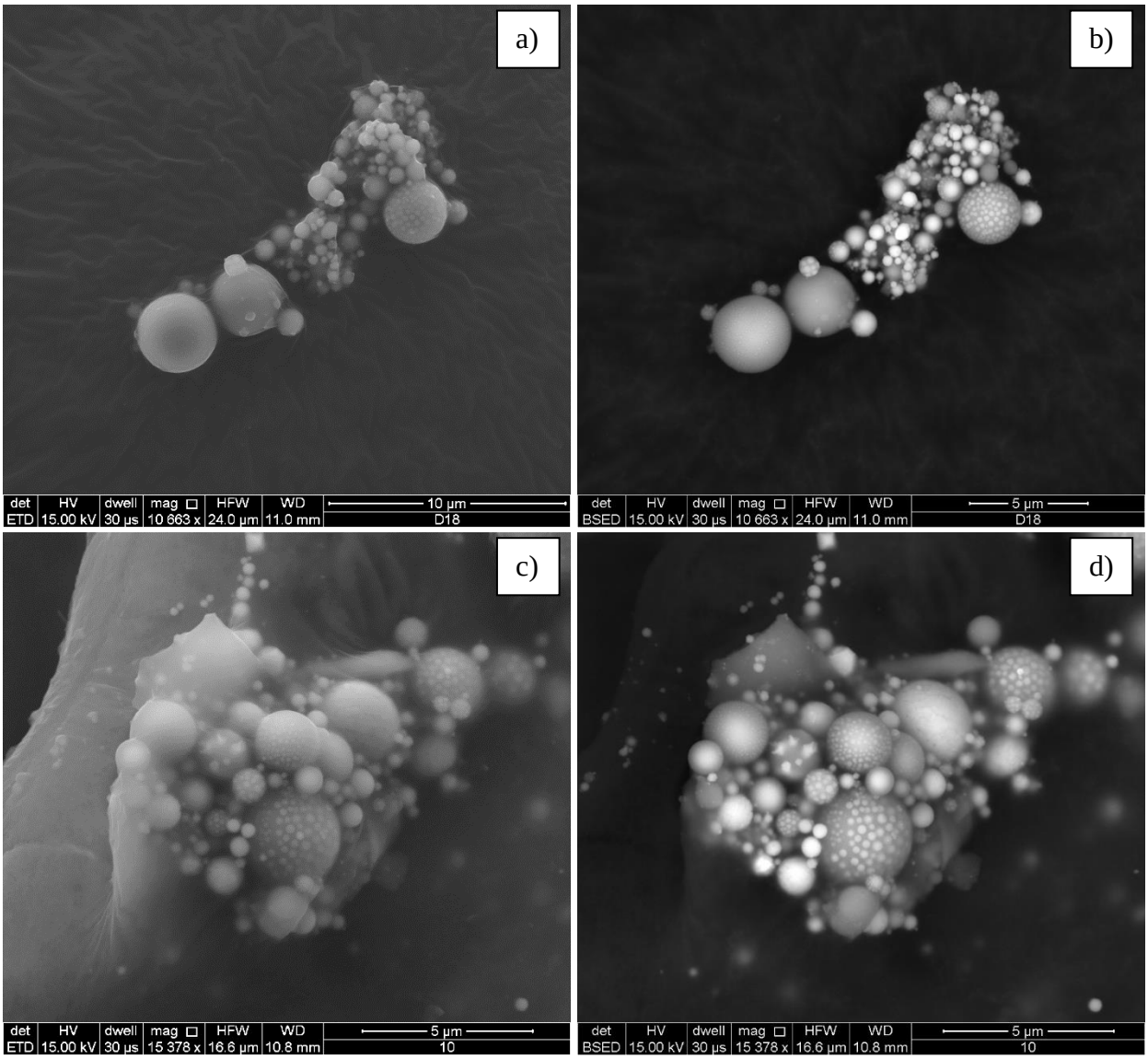

Fig. 8. Example of agglomerates fused smaller particles into a bigger particle found in the ashed sample (a and b) and on filter fiber (c and d) under secondary (a and c) and backscattered (b and d) electron imaging mode.

After categorizing the different type of particles observed in our sample, we determined some conditions for the exclusion of particles to allow a confident particle size analysis of primary formed particles:

- Particles with non-spherical geometry (white arrow on Fig. 9 and 11, possibly representing soil minerals such as silicate or oxide minerals);
- Particles out of focus, particles with a difficult to determine geometry, or particles covered by surrounding particles (peach-color arrow on Fig. 9);
- Fused smaller particles onto the surface of a bigger particle (described in Fig. 7 and also shown with a green arrow on Fig. 9);
- Particle agglomerates (described in Fig. 8 and 11).

Agglomerates were not considered for the particle size distribution analysis via SEM however a brief description of the agglomerates is reported below.

Due to the resolution of the SEM, nm-sized particles (<50 nm) were difficult to identify and image, hence the smaller particle identified had a diameter of 48 nm. Using the MAMA software (reference 1, see Experimental section for details), we tabulated the size of 451 particles that ranged in size from 48 nm to 5.65 µm.

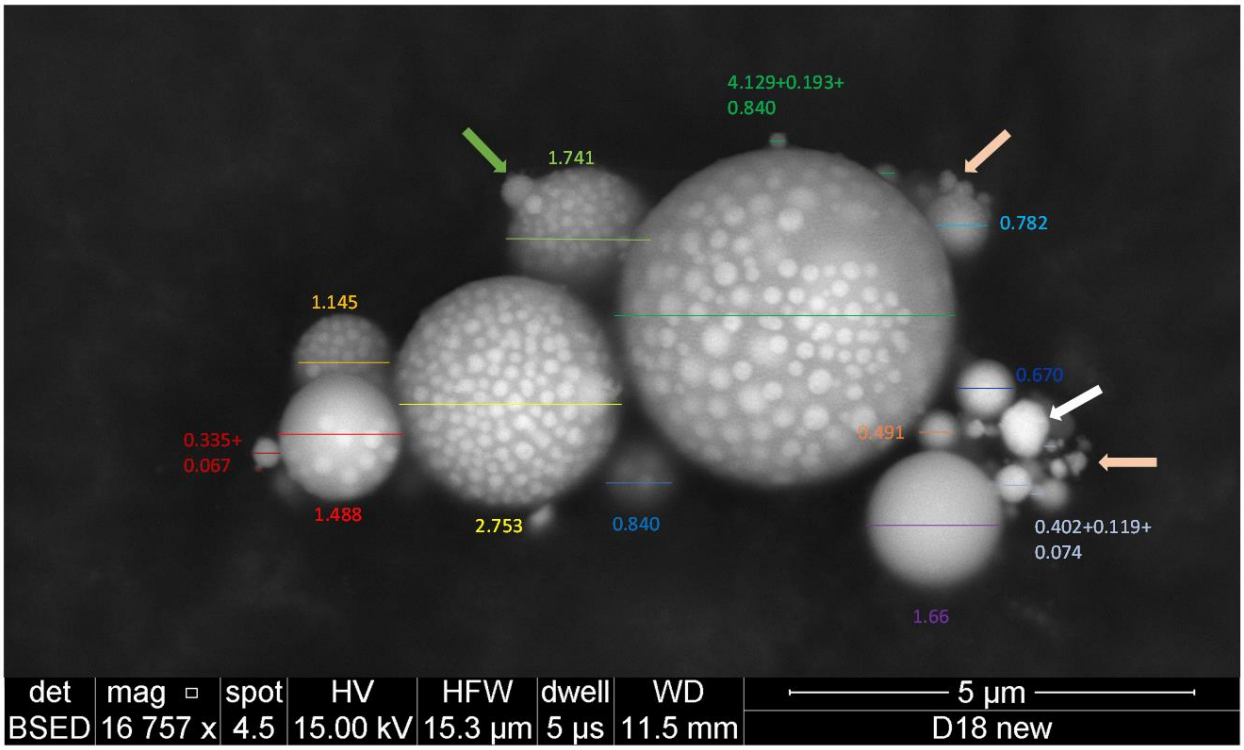

Fig. 9. Backscattered electron image of FLD-20-01-12 particles isolated from filter analyzed for particle size distribution (PSD). Only spherical particles were considered for the particle size analysis. Since the measurement was performed under BSED, the change in contrast is indicative of compositional variation. This figure contains lines on each particle of interest, with their associated color-coded measurements obtained using the ruler in the MAMA software. *Note: the line does not indicate the region considered for particle sizing but represents a way to identify the particles considered for PSD.* The white arrow points to a very bright particle that has facetted edges and thus was not considered for PSD assessment. The peach-colored arrows show multiple small particles that were not sufficiently in focus such that we could determine if they were of interest, and thus were not considered for PSD assessment. The green arrow points to aggregations of spherical particles not considered for PSD.

Particle size analysis considering DLS and SEM measurements

In general, DLS provided particle size distribution in nanometer size range while SEM provides information on particles from 50 nm to micrometer size. As the two methods provide complementary information on sample particles size population, the size distribution of FLD-20-01-12 was computed by determining the number of particles analyzed and their associated size. This was achieved by determining the frequency of the number of particles having the same size in different bins. The bins were chosen as follow: 50 nm bins between 0 and 99 nm, 100 nm bins between 100 and 999 nm, and 1 000 nm bins between 1 000 and 6 000 nm, and results are summarized in Fig. 10.

Overall DLS measurements detected that more than 60% of the particles measured had a diameter < 100 nm with the remaining particles found to range between 778 nm and 5.07 µm. The PSD determined using SEM shows only 4.4% of the particles have a size < 100 nm and the majority of the particles have sizes between 200 nm and 1.69 µm.

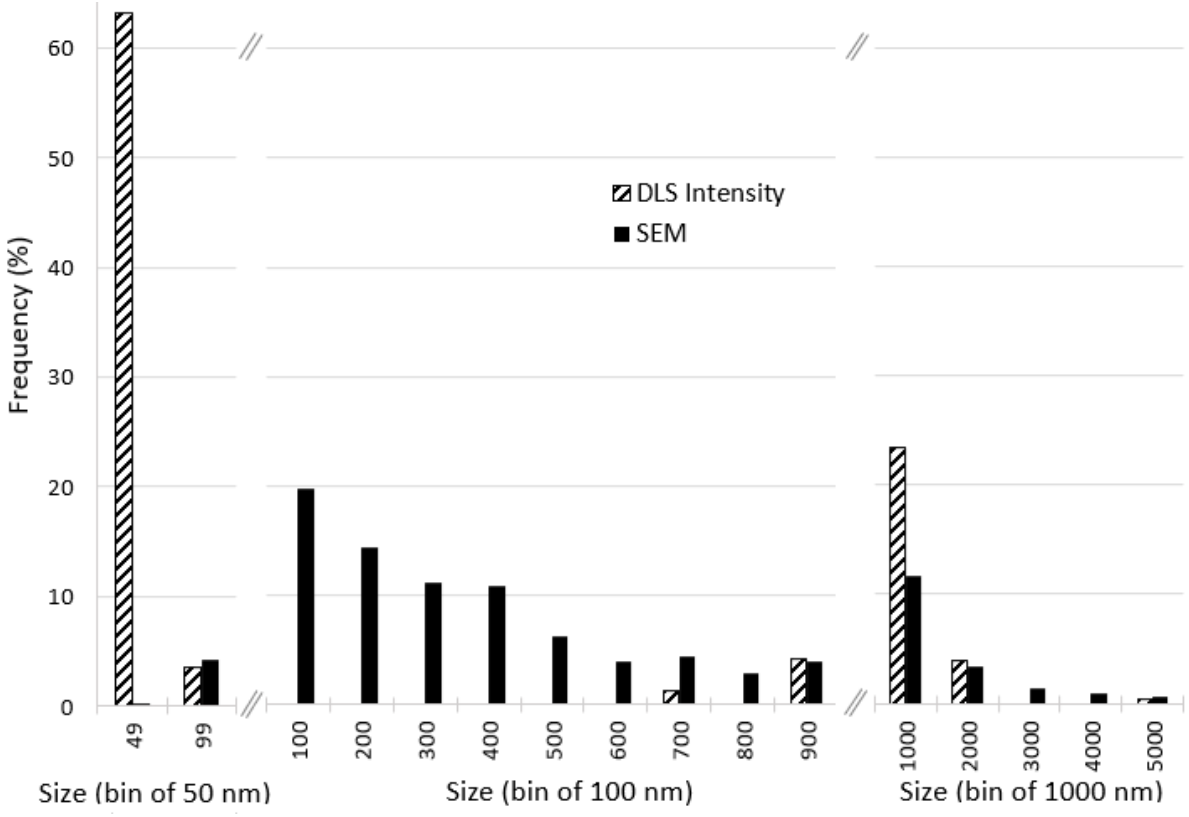

Fig. 10. Particle size distribution of FLD-20-01-12 particles isolated form filter measured using DLS data (reported as number intensity; black patterned histogram) and extracted from SEM images (black solid histogram). The data are represented as the frequency of particle size found in the various bins size. Bin sizes chosen were: 50 nm bins between 0 and 99 nm, 100 nm bins between 100 and 999 nm, and 1 000 nm bins between 1 000 and 6 000 nm.

Agglomerates

Agglomerates were observed in the sample during SEM imaging. These features were not used for the PSD focus of this work, but few images were taken and analyzed are briefly discussed here. Eight agglomerates were analyzed, where we determined the number of particles visible, and the size range of the particles. An example is shown in Fig. 11 of agglomerate #8 and data are summarized in Table 3. It is difficult to determine if these agglomerates represent an artifact of sample preparation (adhesive effects resulting from collection on filter, the effects of later furnace heating, or effects from sample drying) or if they represent particles primary agglomerates formed in the fireball cloud. To determine if agglomerates were formed during sample preparation (furnace heating and samples drying for SEM images) we imaged the particles directly on untreated filters (Fig. 2 and Fig. 8 c and d). The images revealed the presence of agglomerates on the unprocessed filters, confirming that at least some agglomerates were already present in the unprocessed sample.

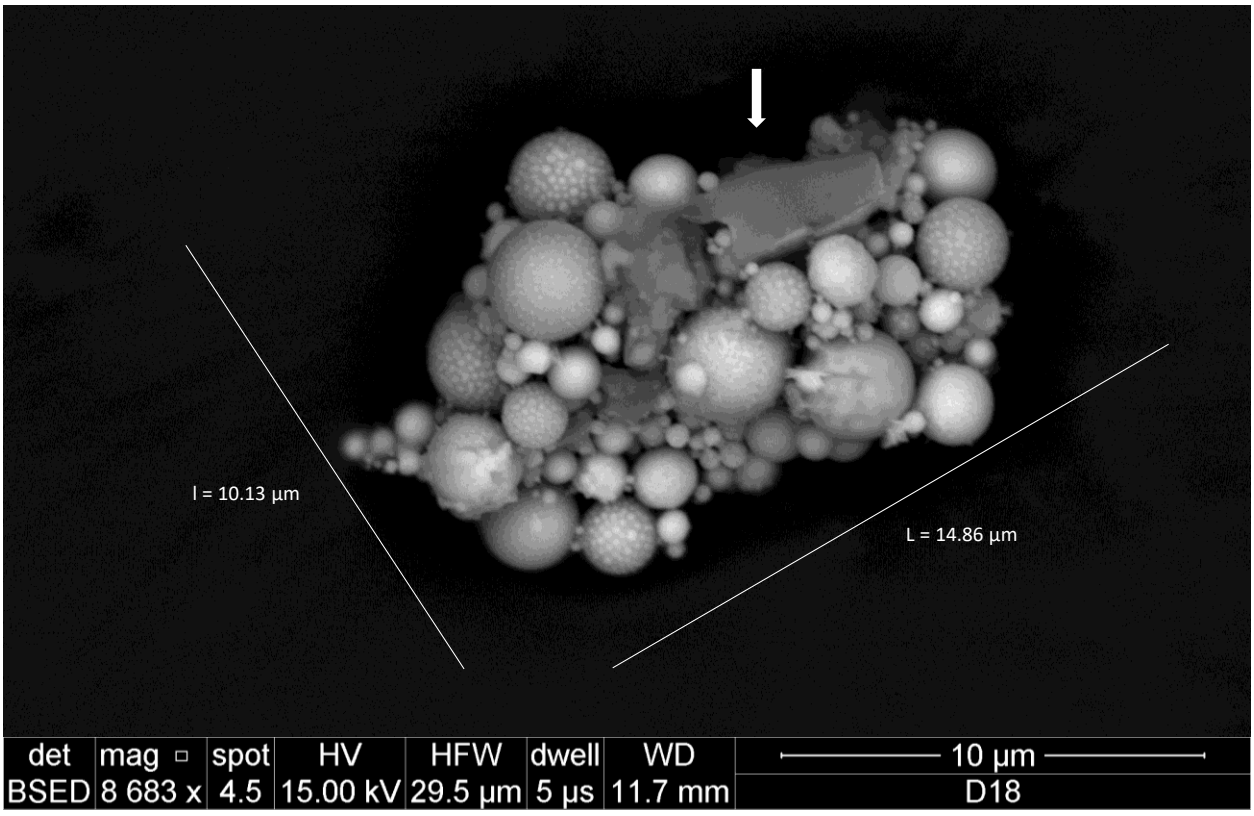

Fig. 11. Backscattered electron image of agglomerated particles (called agglomerate #8 in Table 3), 1 non-spherical grain is present shown with a white arrow. The agglomerate contains a high number of particles and few of were visible and possible to measure with confidence. The sizes of the particles present in this agglomerate range from 96 nm to 2.82 µm. Values in white are the size of the agglomerate; longer length L = 14.86 µm and shorter length l = 10.13 µm.

Table 3. Summary data for FLD-20-01-12 particles observed as agglomerates. Those agglomerates do not seem to be formed during sample preparation (i.e., overlapping of multiple particles) but are fused together. Since no manipulation is possible after deposition of the particles on the carbon tape, only visible particles are counted, but the entire agglomerate probably contains more particles than the ones observed. Since these particles were not the focus of this study only the range of the particle size is given. To have a better idea of the agglomerate size, measurements were done in nm using the ruler in the software giving the longer length of the agglomerate as L and a shorter length as l, as described in Fig. 11.

Name	Number of visible particles	Size particle range in µm	Size agglomerate L x l in nm
Agglomerate #1	23	0.34 – 4.92	14.14 x 7.98
Agglomerate #2	89	0.08 – 3.39	13.06 x 7.04
Agglomerate #3	75	0.11 – 3.46	9.99 x 6.03
Agglomerate #4	76	0.09 – 3.91	10.36 x 6.09
Agglomerate #5	81	0.10 – 4.50	9.23 x 7.33
Agglomerate #6	85	0.12 – 5.14	11.49 x 7.63
Agglomerate #7	124	0.11 – 4.50	1.68 x 9.82
Agglomerate #8	71	0.10 – 2.82	14.86 x 10.13

5. Summary

Particles isolated from a historic US air filter sample were analyzed for chemical spatial distribution, major element composition, and to capture particle size distribution. SEM images and EDS data show that the majority of the sample consists of spherical particles with very few non-spherical particles. The composition of the spherical particles ranges between a Fe-rich and an Al/Si-rich composition as confirmed via chemical analysis via SEM-EDS and IR spectroscopy.

Particle size distribution was conducted using a combination of dynamic light scattering and SEM image analysis. The first method (DLS) is performed on a bulk sample kept in solution, whereas the second method uses analysis of images collected via SEM on dry samples. DLS demonstrate that the particle range in size between ranging 23.4 nm to 5.07 µm. 60% of the particles is in the 0-100 nm range with the remaining particles (isolated and/or agglomerates) identified in the 700 nm to 5.07 µm size range. SEM analysis reveals that particle range in size between 48 nm and 5.65 µm with ~ 55% of the particles identified in the 0-500 nm range. The largest particles are identified in the 600 nm to 5.65 µm size range, similar to what was observed in the DLS measurements.

To determine the particle size distribution in polydisperse samples, such as the one analyzed here, multiple techniques are needed to cover the wide range of particle sizes found in the sample. The use of different analytical techniques to determine PSD however may lead to differences in results mainly related to sample preparation methods and instrumental limitations.

The largest discrepancies in the PSD analysis performed by combining information obtained from DLS and SEM image analysis affects the characterization of particles in the 0-100 nm range. This discrepancy can be explained by the main limitation of SEM in imaging nm-sized particles which are difficult to uniformly focus. Therefore, having data from DLS measurements is important as it allows to obtain PSD data on the 0-50 nm population. However, during DLS analysis larger particle may deposit on the bottom of the cuvette, thus the largest sized population may be underrepresented via DLS. Another limitation of the DLS measurements is that the samples are measures in solution without direct visual on what type of particles the laser is measuring. If the vials or sample become contaminated (for example, with fine dust), the PSD can lead to also erroneous data. As observed on SEM images, few larger agglomerates are also present in such samples. The presence of agglomerates could explain the larger peak observed around 1 000 nm in the PSD diagram for the DLS data (Fig. 10) since the size of these agglomerates are similar to the larger values shown in Table 3. In order to minimize bias on the PSDs from agglomerates, the sample was sonicated prior to analysis. It is not possible at this time to determine if the agglomeration happened during collection, transport, ashing, storing or during the original formation event but the latter option appears to have had some influence. The handling of agglomeration must be considered and articulating in future work addressing particle size distribution and simulation or modeling of such events.

There are limited reports in the literature discussing the chemistry and particle size distribution of materials isolated from air collections of nuclear events. Nathans et al. (reference 4), measured size distribution of particles collected on air filters of airburst events from the Dominic series 1962. The particles identified ranged in size from 0 nm to <1500 nm (no exact range was given other than lower and upper boundaries 26 nm and 1 490 nm), with a mean diameter ranging from 65 nm to 210 nm depending on the event analyzed. On average Nathans identifies that 30% of particles have a diameter included between 0-100, and about 35-40% of particle range from 100 nm and 500 nm considering all events under study. Overall, our measurements of particle size are in broad agreement with Nathans et al.

Modern characterization of historic fallout particulate samples can provide new information on particulate nucleation and particle growth from the vapor phase and help determine how radionuclides are incorporated in macro-sized debris such as aerodynamic fallout.

6. References

1. B. K. Gaschen, J. J. Bloch, R. Porter, C. E. Ruggiero, D. A. Oyen and K. M. Schaffer. “MAMA User Guide v2.0.1”. LANL Report LA-UR-16-25116, 2016. Web. doi:10.2172/1291192.
2. C. F. Snyder and A. T. Hattenburg. “Refractive indices and densities of aqueous solutions of invert sugar” National Bureau of Standards, Monograph 64, 1963.

3. J. F. Swindells, C. F. Snyder, R.C. Hardy and P.E. Golden. “Viscosities of sucrose solutions at various temperatures: Tables of recalculated values”. Supplement to National Bureau of Standards, Circular 440, 1958.
4. M. W. Nathans, R. Thews, W. D. Holland, and P. A. Benson. “Particle size distribution in clouds from nuclear airbursts”. Journal of Geophysical Research, 75 (36), 7559-7572, 1970.